Earth and Planetary Science Letters 595 (2022) 117769

Contents lists available at ScienceDirect

Earth and Planetary Science Letters

www.elsevier.com/locate/epsl

Trace elements in olivine fingerprint the source of 2018 magmas and shed light on explosive-effusive eruption cycles at Kīlauea Volcano

Adrien J. Mourey [a,*], Thomas Shea [a], Kendra J. Lynn [b], Allan H. Lerner [c], Sarah Lambart [d], Fidel Costa [e], Jeffrey Oalmann [f], R. Lopaka Lee [b], Cheryl Gansecki [g]

[a] Department of Earth Sciences, University of Hawai'i at Mānoa, HI, United States
[b] U.S. Geological Survey Hawaiian Volcano Observatory, HI, United States
[c] Department of Earth Sciences, University of Oregon, OR, United States
[d] Department of Geology and Geophysics, University of Utah, Salt Lake City, UT, United States
[e] Institut de Physique du Globe de Paris, France
[f] Asian School of the Environment, Nanyang Technological University, Singapore
[g] Geology Department, University of Hawai'i at Hilo, United States

ARTICLE INFO

Article history:
Received 2 May 2022
Received in revised form 12 July 2022
Accepted 6 August 2022
Available online xxxx
Editor: C.M. Petrone

Keywords:
Kīlauea
olivine
trace elements

ABSTRACT

Understanding magma genesis and the evolution of intensive parameters (temperature, pressure, composition, degree of melting) in the mantle source of highly active volcanic systems is crucial for interpreting magma supply changes over time and recognizing cyclic behavior to anticipate future volcanic behavior. Major and trace elements in olivine are commonly used to study variations in mantle lithologies and melting conditions (e.g., temperature, pressure, oxygen fugacity) affecting the mantle over time. Here, we track the temporal evolution of primary melts through the most recent cycle of explosive and effusive eruptions at Kīlauea (Hawai'i), which spans the last ~500 years. We report major and trace elements in olivine from the last explosive period (~1500 – early 1820's Keanakāko'i Tephra) and the most recent decade of the current effusive period (2018 LERZ, 2015–2018 Pu'u'ō'ō, 2008–2018 lava lake and 2020 eruption in Halema'uma'u). Scandium concentrations in olivine allow characterizing changes in mantle source between 1500 and 2018, and suggest that the recent (2015–2018) magma feeding the Pu'u'ō'ō cone did not significantly interact with the magma that erupted in the LERZ in 2018. The evolution of olivine and melt compositions over the past 500 years is not easily reconcilable with variations in mantle potential temperature, pressure of mantle melt pooling and storage, or oxygen fugacity. Instead, Sc, Mn, and Co concentrations and Ni/Mg ratio in high forsterite (Fo >87) olivine advocate for an increase in the proportion of clinopyroxene in the mantle source associated with a slightly higher degree of partial melting from 1500 to 2018. Changes in primitive melt compositions and degrees of mantle melting may well modulate magma supply to the crust and formation-replenishment of steady or ephemeral summit reservoirs, and thereby control transitions between explosive and effusive periods at Kīlauea. Analyzing trace elements in olivine at Kīlauea and elsewhere could therefore provide important clues on subtle changes occurring at the mantle level that might herald changes in volcanic behavior.

1. Introduction

Kīlauea is an active shield volcano located on the Island of Hawai'i (Fig. 1), iconic for its vigorous effusive activity over the last 200 years (Poland et al., 2014). However, several centuries-long periods of explosive activity have also occurred over the past 2500 years (Swanson et al., 2014). Kīlauea's last explosive phase (~1500 – early 1820's) produced the Keanakāko'i Tephra (KT), a period over which magma supply and eruption rates are inferred to be low (5×10^{-4} km^3/yr) compared to the 20th (up to 0.1 km^3/yr) and 21st centuries (0.1–0.2 km^3/yr; Poland et al., 2014). The long-lived KT sequence was produced by over ~320 years of dominantly explosive eruptions, following the collapse of the modern Kīlauea caldera at around 1500 ± 30 C.E. (Swanson et al., 2012). The KT is composed of explosive phreatomagmatic, phreatic, and high lava fountain deposits, as well as one lava flow (McPhie et al., 1990; Swanson et al., 2012). During explosive periods at Kīlauea, magma is thought to erupt with little to no processing

* Corresponding author.
E-mail address: amourey@hawaii.edu (A.J. Mourey).

https://doi.org/10.1016/j.epsl.2022.117769
0012-821X/

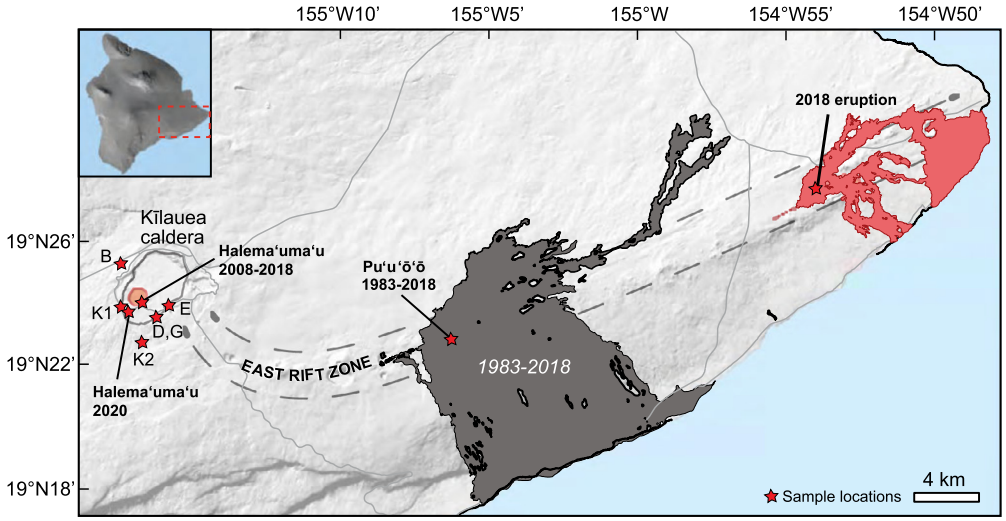

Fig. 1. Map of Kīlauea Volcano with the studied eruptions. Inset: Map of the Island of Hawai'i. Letters B, D, E, G, K1 and K2 correspond to the unit name for the KT eruptions. Red circle inside the caldera is the Halema'uma'u lava lake before the 2018 eruption. (For interpretation of the colors in the figure(s), the reader is referred to the web version of this article.)

in the crust (Sides et al., 2014; Lynn et al., 2017), whereas during the current effusive period, summit reservoirs are stable and steadily replenished (Poland et al., 2014; Lynn and Swanson, 2022). Following the KT period, from 1840 to 1959, magma supply and the degree of partial melting remained low (Pietruszka and Garcia, 1999). Since 1959 and through the present day, eruption rates and magma supply have been steadily increasing (Poland et al., 2014; Wright and Klein, 2014). Between 2003 and 2007, a significant increase in the CO_2 emissions and inflation at Kīlauea's summit also suggested an additional surge in mantle-driven magma supply (Poland et al., 2012). Kīlauea is therefore currently undergoing a high magma supply period within a largely effusive cycle.

The transition between effusive and explosive periods is thought to be punctuated by major caldera forming events, with smaller to moderate caldera collapse events in between (<km in scale; Swanson et al., 2014). In addition to the caldera collapse in 1500, several other collapses occurred in 1790 (inferred collapse event), 1832, 1840, 1868 (Brigham, 1909) and 1924. These collapse events are known to strongly perturb Kīlauea's crustal plumbing system (Anderson et al., 2019). The last significant caldera collapse occurred in 2018 during the lower East Rift Zone (LERZ) eruption, the largest eruption in the last 200 years of activity (Neal et al., 2019). Prior to the 2018 crisis, Kīlauea Volcano was erupting at two locations, Pu'u'ō'ō on the East Rift Zone (ERZ), and within a lava lake inside Halema'uma'u crater at the summit. The large cumulative volume of the Pu'u'ō'ō lavas between 1983–2018 (>4 km^3) was sustained by a nearly continuous supply of mantle-derived magma that mixed with large volumes of stored summit magmas (Neal et al., 2019). During this period, Kīlauea erupted near-continuously at the middle ERZ (Fig. 1) at the Pu'u'ō'ō cone. On April 30th 2018, the configuration of the shallow magmatic storage system changed after complete drainage of both the Halema'uma'u lava lake and the Pu'u'ō'ō vent (Neal et al., 2019). The LERZ 2018 eruption was preceded by swarms of lower-crustal earthquakes 5–13 km beneath Kīlauea's summit area that started six months before the onset of the eruption that have been interpreted either as an increase in magma supply and pressurization of the summit area (Flinders et al., 2020), or as backing up of magma from a blocked shallow Pu'u'ō'ō plumbing system (Patrick et al., 2020). The eruption was split into three main eruptive phases based on field observations and lava geochemistry (Gansecki et al., 2019). Phase 3 (lavas from the Ahu'ailā'au or fissure 8 vent) was by far the most voluminous (>92% of the total LERZ 2018 eruption volume) and the most destructive, emitting hot, low-viscosity mafic lavas (bulk MgO ~7–9.5 wt.%, Gansecki et al., 2019). Highly variable bulk compositions between different fissures showed that mixing between a volumetrically dominant mafic magma and two more evolved magmas (high-Ti basalt and andesite) occurred. Although it is likely that the evolved magmas were stored somewhere in the ERZ for decades (Neal et al., 2019), the origin of the mafic magma is still uncertain (summit reservoirs vs. Pu'u'ō'ō vs. deep East Rift Zone; Gansecki et al., 2019; Wieser et al., 2021; Lerner et al., 2021a; Pietruszka et al., 2021). However, identifying the underground source(s) of magma that fed the 2018 Kīlauea LERZ eruption is critical for recognizing areas most prone to signs of pre-eruptive unrest.

Locating magma sources at Kīlauea Volcano (Hawai'i) is challenging given the complex and laterally extensive magmatic plumbing system. Mantle melts feed a suite of connected deep (3–5 km) and shallow (~1 km) summit reservoirs, the South Caldera and Halema'uma'u reservoirs respectively, which then distribute magmas to the Southwest and East Rift Zones (Fig. 1; Poland et al., 2014). Summit reservoirs and the upper/middle ERZ were activated seismically and geodetically prior to and during the 2018 LERZ eruption (Neal et al., 2019). Because the different Kīlauea reservoirs (Pu'u'ō'ō, Halema'uma'u, and phase 3 from the LERZ 2018 eruption) have similar bulk and matrix glass major-element compositions (i.e., glasses with ~11 wt.% CaO and ~4.9–7.2 wt.% MgO; Gansecki et al., 2019; Lerner et al., 2021a), and largely indistinguishable trace elements (i.e., same Nb/Y ratios between 2018 LERZ phase 3 and 21st century summit and rift zone lavas; Pietruszka et al., 2021), identifying the origin of the 2018 LERZ magma on the basis of geophysics and major/minor element chemistry is difficult. The complete draining of lava from both the Pu'u'ō'ō vent and the Halema'uma'u lava lake shortly before and during the eruption support a well-connected plumbing system and thus a potential contribution from both summit reservoirs and Pu'u'ō'ō. In addition, CO_2-H_2O vapor saturation pressures derived from olivine-hosted melt inclusions from the 2018 eruption (Lerner et al., 2021a; Wieser et al., 2021) indicate relatively shallow trapping at 1–5 km depth, consistent with the location of the summit reservoirs. These depths are, however, also consistent with crystallization of olivine under Pu'u'ō'ō or the rest of the ERZ. Moreover, total SO_2 emissions measured during the LERZ 2018 eruption suggest that the erupted volume was around twice the modeled volume loss from the shallow Halema'uma'u reservoir

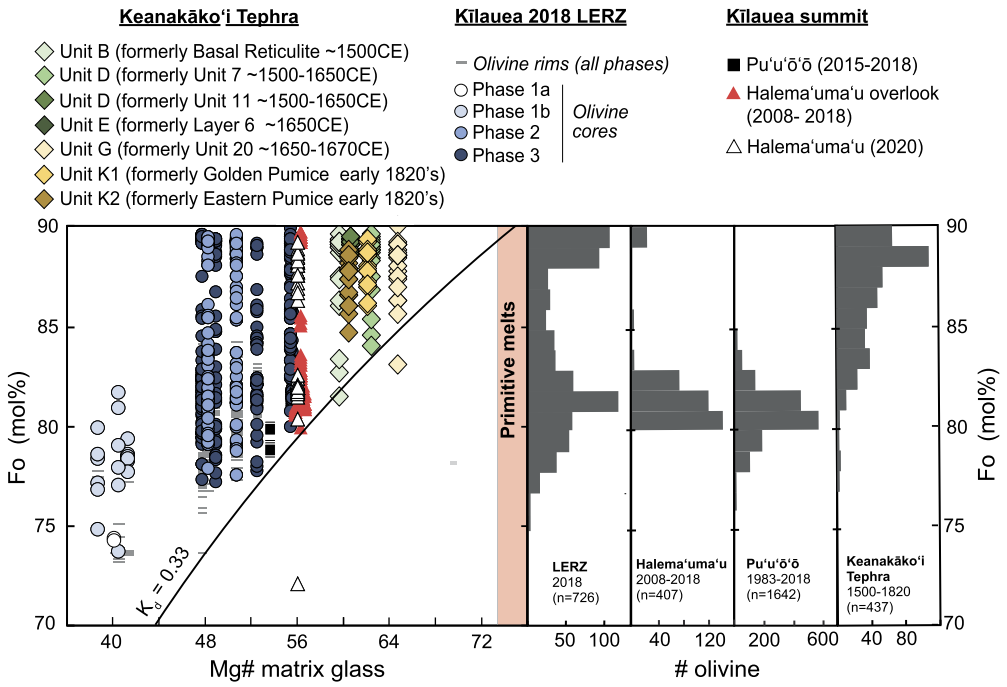

Fig. 2. Olivine compositions and olivine-melt equilibrium. Olivine Fo composition for the KT (cores), 2008–2018 Halema'uma'u (cores), 2020 Halema'uma'u (cores), 2015–2018 Pu'u'ō'ō (cores), and 2018 LERZ (cores and rims) samples. Equilibrium olivine Fo content is calculated with the matrix melt composition and a melt-olivine Mg/Fe exchange coefficient (K_d) of 0.33 (Putirka, 2016). Fe^{3+}/Fe_T was fixed at 0.18 to calculate Mg# of matrix glasses (Moussallam et al., 2016; Lerner et al., 2021b). KT olivine and glasses major compositions are from Lynn et al., 2017. Other Kīlauea olivine and matrix glasses data (except for the 2018 LERZ eruption) are from Sides et al., 2014.

(Anderson et al., 2019; Kern et al., 2020), implying that at least one other reservoir (potentially the South Caldera) contributed to the eruption. The partial overlap in Fo (= Mg/(Mg+Fe) mol%) between the 2018 LERZ and recent Pu'u'ō'ō olivine (Gansecki et al., 2019) may correspond to a transitional phase where the Pu'u'ō'ō magma was being flushed out from the rift system and then mixed with magma arriving from the summit reservoir. High-Fo olivine (Fo_{87-89}), however, was also erupted in 2018 (Fig. 2) and having not been seen in the East Rift Zone at Kīlauea since the 1969–74 Maunaulu eruption (Gansecki et al., 2019; Lynn and Swanson, 2022), but high-Fo olivine is sometimes found during the 2008–2018 Halema'uma'u lava lake period. Over the last 500+ years, this high-Fo olivine population appears in the absence of a volumetrically significant stable reservoir that do not mix efficiently recharge magmas after Kīlauea caldera collapses (Lynn and Swanson, 2022). Prior to the 2018 summit collapse, Pu'u'ō'ō had evolved olivine (Fo_{78-80}) coming from a mature and buffered summit reservoir (Lynn and Swanson, 2022), indicating that high-Fo olivine observed in phase 3 LERZ magmas in 2018 were generated from at least one additional source other than Pu'u'ō'ō.

The first objective of this paper is to better constrain the origin of the voluminous mafic magma from phase 3 of the 2018 LERZ eruption. Traditionally, bulk rock trace element compositions are used to constrain the mantle melting conditions and its chemistry. However, mantle melt composition and properties can be overprinted by magma mixing, crystallization and assimilation during storage and ascent prior to an eruption. Therefore, we use the chemical composition of olivine crystals from Pu'u'ō'ō, Halema'uma'u and 2018 LERZ lavas to fingerprint the different magmas and identify which magma reservoirs were involved in the 2018 LERZ eruption. The renewed presence of high-Fo olivine in 2018 also affords a longer-term analysis of potential changes in the characteristics of primitive magmas over the last 500 years and the last explosive-effusive cycle. We leverage major and trace elements from primitive (high-Fo) olivine macrocrysts from a low magma supply period (KT 1500 – early 1820's) and from recent eruptions of the current high magma supply period (2018 LERZ, 2015–2018 Pu'u'ō'ō, 2008–2018 Halema'uma'u and 2020 Halema'uma'u eruptions) to characterize long-term changes in primary melts at Kīlauea. Thus, a second objective of this work is to explore potential petrogenetic links between the nature of primitive melts in the mantle and the occurrence of long-lived effusive or explosive cycles at Kīlauea.

2. Methods

From 2008 to 2018, a lava lake was present within Halema'uma'u crater, located in the southwest area of the summit caldera (Fig. 1). We examined 9 samples from this lava lake collected by scientists at the U.S. Geological Survey's Hawaiian Volcano Observatory HVO (wafted Pele's hairs and tears, tephra) near the old Halema'uma'u parking lot between 2008 and 9 May 2018. On 20 December 2020, eruptive activity returned to Halema'uma'u and limited tephra samples were deposited south of Halema'uma'u crater. We studied one sample (in which only two microphenocrysts were large enough to analyze by laser ablation) from this last summit eruption (sample KS20-525). All summit samples consist of juvenile Pele's hair, tears, ash and lapilli that were naturally quenched in air. These samples are glassy and the proportion of olivine phenocryst is <5 vol.% (bubble-free volume).

Olivine crystals were collected from juvenile material in deposits spanning the entire KT period (1500 – early 1820's, see descriptions in Swanson and Houghton, 2018). The KT units investigated (Fig. 1) include unit B (~1500 C.E., formerly the Basal Reticulite), unit D (two pumice-rich samples, formerly units 7 and 11 from S07-39, ~1500–1650 C.E.), unit E (~1650 C.E., formerly the layer 6 scoria, unit G (formerly unit 20 from S07-39, ~1650–1670 C.E., a pumice-rich layer), unit K1 (between 1790 and early 1820's, formerly the Golden Pumice), and unit K2 (between 1790 and early 1820's, formerly the Eastern Pumice).

Samples from the 2018 eruption are mainly spatter or rapidly quenched lavas that were collected from the early phase 1 (re-

ferred to as phase 1a, erupted 3 to 9 May 2018; Gansecki et al., 2019), late phase 1 (referred to as phase 1b, erupted 12 to 18 May 2018), phase 2 (erupted 17 to 27 May 2018) and phase 3 (erupted 28 May to 4 August 2018).

Finally, we also study two samples from the Pu'u'ō'ō eruption collected in 2015 during episode 61 and in April 2018. We chose to focus on the last stages of this eruption since they would be most relevant to the compositions possibly involved in the 2018 LERZ events.

2.1. Electron probe micro-analysis (EPMA)

Major and minor element composition of the matrix glasses and olivine were determined using a JEOL JXA-8500F Hyperprobe with five wavelength-dispersive spectrometers at the University of Hawai'i. Olivine spot analyses were done using a 20 keV accelerating voltage, 200 nA beam current, and with a diameter of 10 µm. Peak counting times were 40 s for each element. San Carlos USNM 111312/444 and Springwater UNSM 2566 olivine were used as internal standards for Si, Fe and Mg, a CalTech Ni-ol for Ni, Kakanui augite USNM 122142 for Ca, Chromite USNM 117075 for Cr, Verma garnet for Mn and A99 basalt glass (USNM 113498/1) for P. For glass analyses, an accelerating voltage of 15 keV, a current of 10 nA and a beam diameter of 10 µm were used. Peak counting time was 40 s for each element. A99 basalt glass (USNM 113498/1) was used for Si, Al, Fe, Mg, Ca, Sphene glass for Ti, Verma garnet for Mn, Amelia albite for Na, Orthoclase (OR-1) for K, fluor-apatite USNM 104021 for P. VG-2 was used as an external standard.

2.2. Laser ablation inductively coupled plasma mass spectrometry (LA-ICPMS)

Trace element analyses were measured in olivine and matrix glass at the Earth Observatory of Singapore using a Photon Machines Analyte G2 193 nm Ar-F excimer laser with a two-volume ablation cell coupled to a Thermo-Scientific Element 2 ICP-MS. Sample aerosol was transported from the ablation site in He gas with a total flow rate of 1 L/min and mixed with 1.0 L/min of Ar gas ~15 cm upstream from the plasma using a glass mixing bulb. For the 2008–2020 samples in this study, the ICP was sustained with an RF Power of ~1500 W. A spot size of 80 × 80 µm (square), fluence of 3.55 J/cm^2, and a repetition rate of 10 Hz was used for matrix glass and olivine analyses.

Total counting times were 5 ms for ^{29}Si on olivine and ^{44}Ca on matrix glass and 10 ms for all other isotopes. For the KT olivine, analyzed during a previous session, the laser was run at 70% output, 5.9 J/cm^2 fluence, and frequency of 8 Hz with constant voltage with a spot size of 50 x 50 µm (square). Data reduction was performed using the Trace Elements IS data reduction scheme of Iolite v. 3.6 (Paton et al., 2011). For all 2008–2020 analyses, the synthetic basaltic glass GSD-1G was used as the primary calibration standard, whereas NIST 612 was used for the KT analyses. Precision and accuracy of secondary standards (BCR-2G, BHVO, NIST) are reported in the Supplementary tables.

3. Results and discussion

3.1. Pathways of the magma supplying the 2018 Kīlauea eruption: implications for the recent plumbing system of Kīlauea Volcano

The 2018 LERZ lavas contain heterogeneous olivine core compositions (phase 1 with Fo_{73-82}, phases 2 and 3 with Fo_{77-90}), a much broader range than the lower-Mg, homogeneous olivine compositions erupted in the last decade at Pu'u'ō'ō (Fo_{78-80}) or Halema'uma'u (Fo_{80-82}, rarely to Fo_{90}) (Fig. 2). Olivine core compositions in samples from all phases of the 2018 eruption are generally out of Fe-Mg equilibrium with the host melt ($K_{Fe^{2+}-Mg^{2+}}^{ol/melt} \sim$ 0.33 with 'K' the crystal/melt distribution coefficient; Putirka, 2016; Matzen et al., 2011) (Fig. 2). In contrast, recent Pu'u'ō'ō and some Halema'uma'u olivine crystals (with Fo_{80}) are nearly in equilibrium with their carrier melts. Most of the olivine from the 2018 LERZ eruption are normally zoned (decreasing Fo from core to rim; Fig. 3). This zoning is inferred to have developed during incorporation and mixing of the higher-Fo olivine cargo with a more evolved melt either at the summit or in the ERZ (Gansecki et al., 2019).

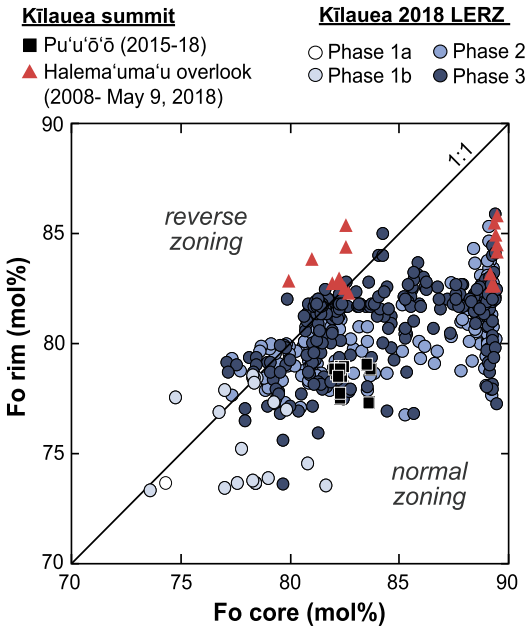

Fig. 3. Forsterite content in olivine (rims and cores) of recent Kīlauea eruptions. The 1:1 line represents olivine with no zonation. Most of the olivine (>95%) from the 2018 LERZ eruption have normal zoning. Olivine from the Halema'uma'u lava lake have rims slightly higher in Fo (Fo_{82-85}) compared to the olivine from LERZ 2018. Pu'u'ō'ō olivine are unzoned or slightly normally zoned.

The presence of primitive olivine (Fo_{87-90}, Fig. 2) at Kīlauea requires fluxes of MgO-rich melts into the reservoirs (Helz et al., 2014). High-Fo (Fo_{87-90}) olivine has been infrequently erupted during the modern high-effusion-rate period, mainly with Kīlauea Iki 1959 and Maunaulu 1969–1974 lavas. They were, by contrast, recurrent in tephra and lavas from the KT period. Fo_{87-89} olivine is thought to form at mid-crustal levels, where water-poor, primitive melts with densities of 2.8 – 2.9 g/cm^3 are neutrally buoyant (Putirka et al., 2018). These primitive melts, and their high-Fo olivine cargo, would periodically intrude the summit reservoirs, a scenario consistent with the normal Fe-Mg zoning in most (>95%) olivine erupted in 2018 (Fig. 3). By contrast, low-moderate Fo olivine (Fo_{78-83}) typifies the 35 year-long Pu'u'ō'ō period as well as the recent lava lake period at the summit. Even though extensive processing within the crust over several years could obliterate high-Fo cores to lower Fo (Gleeson and Gibson, 2019), the overall smaller size of Pu'u'ō'ō olivine in comparison with the 2018 LERZ olivine indicate that these low Fo compositions may reflect the volumetrically large and persistent set of summit reservoirs, where most of the recent olivine crystallizes. Lower Fo_{73-77} olivine would dominantly crystallize in more fractionated and cooler magmas residing within the ERZ.

The origin of the 2018 LERZ mafic phase 3 magma cannot be easily determined using only major elements (Fe-Mg) in olivine because of the large compositional overlap between potential source reservoirs (Figs. 2 and 3). Trace elements, particularly those that do not vary significantly in olivine during fractionation, can shed more light on source characteristics. For instance, Sc is moderately incompatible in olivine and increases with decreasing Fo (Fig. 4a).

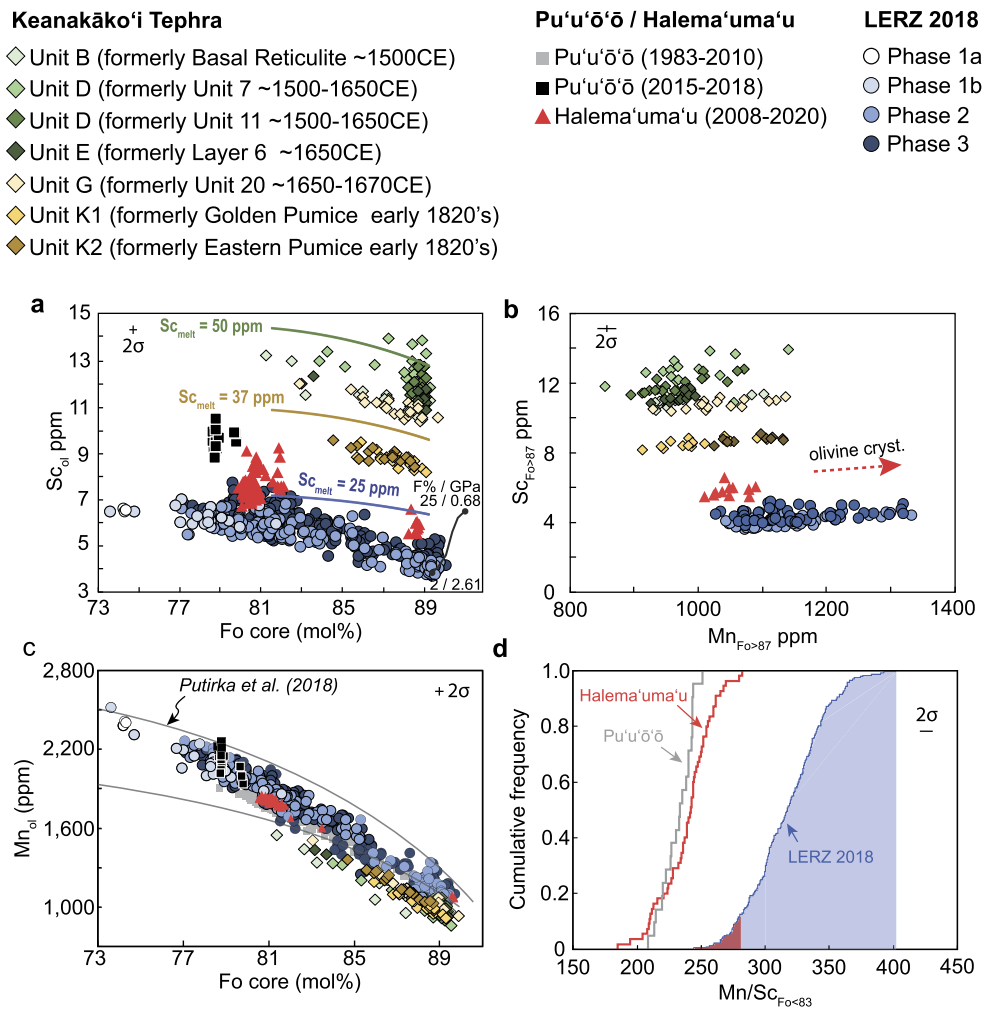

Fig. 4. Major (Fe-Mg) and trace (Mn, Sc) elements in olivine from the KT units, 2015–2018 Pu'u'ō'ō, 2008–2018 Halema'uma'u, 2020 Halema'uma'u, and the 2018 LERZ eruption at Kīlauea. (a) Sc versus Fo content. Melts in equilibrium with Fo_{81-90} olivine only fractionate olivine (Sc is incompatible in olivine). The black curve models olivine compositions in equilibrium with 5–40% melts of peridotite (Nikkola et al., 2019) evolving with the degree of partial melting in percent ($F\%$) and melt aggregation pressures in GPa. Higher Sc contents in olivine from the KT units cannot be modeled with the same mantle composition as for the 2018 LERZ olivine and require a change in the source composition. Fractional crystallization models (blue, orange and green curve) show changes in Sc and Fo in olivine during fractional crystallization as a function of Sc concentration in the starting melt. Higher Sc concentration (up to 50ppm) in primitive melts could explain the measured variations in Sc. The model is based on that presented in Lynn et al. (2017) where Fe-Mg partitioning is calculated using a $K_d = 0.33$ and a partition coefficient D_{Mg} from Putirka et al., 2008. The melt-olivine Sc partition coefficient is taken to be 0.25 (Beattie et al., 1991; Spandler and O'Neill, 2010). (b) Sc vs. Mn in primitive olivine (Fo>87). Mn increases during magma fractionation. (c) Mn vs. Fo content in olivine cores. Mn in-Ol fractionation trends for low- and high-Fo olivine are from Putirka et al., 2018. The trends cannot reproduce the lowest Mn-in ol data, arguing for different primitive melt compositions during the KT period. (d) Cumulative frequency plot of Mn/Sc values in $Fo_{<83}$ olivine. This ratio helps to discriminate olivine from the recent Pu'u'ō'ō (2015–2018) or Halema'uma'u (2008–2020) from the LERZ 2018 olivine. The red and blue areas for the LERZ 2018 olivine highlight the potential contribution from Pu'u'ō'ō and Halema'uma'u (<10%), and from the South Caldera reservoirs (>90%), respectively.

Compared to Fe-Mg, Sc may also diffuse more slowly (i.e., tri- and tetravalent trace element diffusivities being lower than that of divalent elements; Putirka et al., 2018), although other data suggests Sc may diffuse at rates comparable to divalent cations (Spandler and O'Neill, 2010; Bouvet de Maisonneuve et al., 2016). Alternatively, Sc may be subject to trace element coupling (e.g., Lynn et al., 2020) and stay effectively locked in the olivine lattice. In either case, initial Sc concentrations may be better preserved through time. These characteristics (incompatible behavior, potentially slow diffusivity or permanency associated with coupling) make Sc an efficient tracer of liquid or source composition. Sc concentrations in Fo_{78-80} Pu'u'ō'ō olivine (9–11 ± 0.3 ppm, Fig. 4a) are significantly higher than Fo_{78-80} olivine from the 2018 LERZ eruption (6–8 ± 0.3 ppm). Halema'uma'u olivine have Sc concentrations slightly higher than the 2018 LERZ olivine (Fo_{88-90} with Sc=5.5–6.6 ppm and Fo_{80-82} with Sc=6.4–9.3 ppm). Preliminary data in two Fo_{82} olivine from the 2020 Halema'uma'u eruption yield Sc concentrations similar to previous Halema'uma'u olivine (7.7–8.2 ppm) for the same Fo content. The partition coefficient of Sc between olivine and the melt stays constant around 0.25 between FMQ −2 and +2 (Mallmann and O'Neill, 2009). Hence, a change in the oxidation state cannot explain the difference in Sc between Pu'u'ō'ō and LERZ 2018 olivine (Fig. 4a). Therefore, variations in parental melt compositions - brought about by changes in source composition, melting T and P - are most likely the primary control over olivine Sc contents.

Fractional crystallization of Kīlauea basaltic melts affects Sc concentration in olivine only moderately and in a predictable fashion that cannot lead to the differences in Sc observed between recent Pu'u'ō'ō and LERZ 2018. Instead, Sc data indicate that the magma source of the Pu'u'ō'ō olivine must be richer in Sc than the summit source, and ultimately, that the recent Pu'u'ō'ō olivine cargo never made it to the LERZ 2018 eruption site. Therefore, magma feeding the Pu'u'ō'ō vent in the years preceding 2018 did not interact significantly with the magma erupting at the LERZ, and was perhaps stored somewhere in the rift zone after the collapse

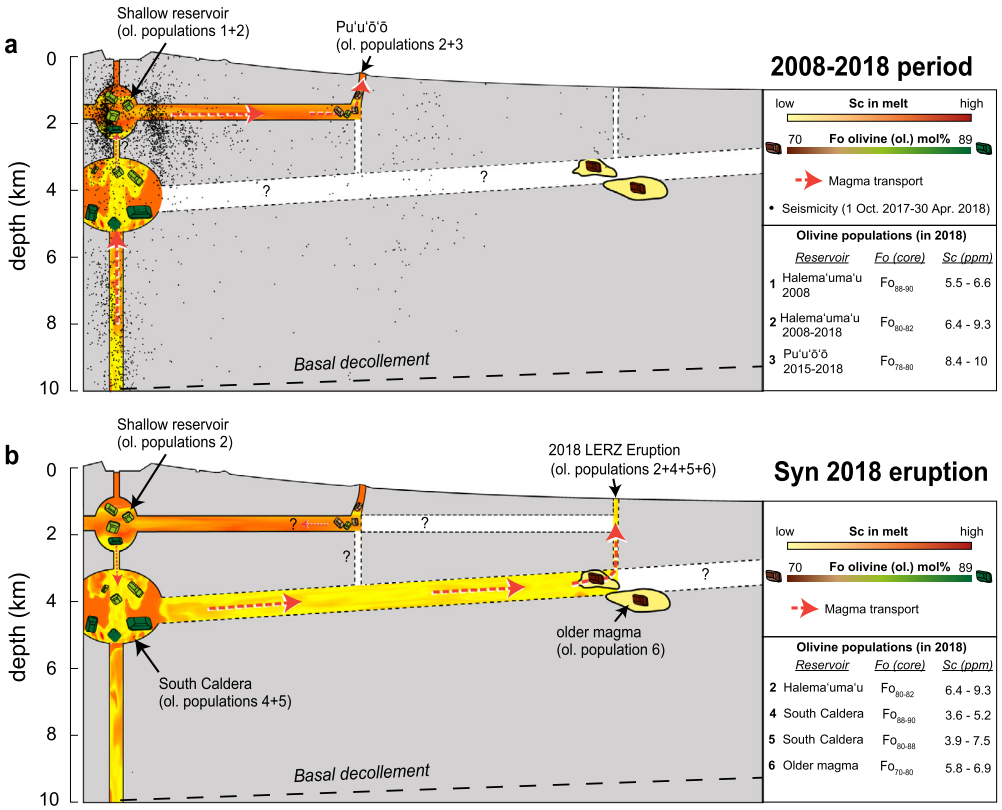

Fig. 5. Summary of key components of the plumbing system under Kīlauea (modified from Wieser et al. (2021) before (a) and during (b) the 2018 LERZ eruption, and the range in olivine composition (Fo=forsterite and Sc content) in the different magmatic reservoirs. The olivine populations are based on differences in Fo and Sc contents. Sc content in olivine implies that the low- and high-Fo populations are present in both the shallow and deep summit reservoirs, but have significant differences in Sc contents (lower Sc contents in the South Caldera reservoir). Earthquakes (black dots; all magnitudes earthquakes from the HVO database) in the six months prior to the 2018 LERZ eruption suggest magma intrusions preceding the 2018 eruption. Earthquake clusters at 5–13 km depth, below the deeper South Caldera reservoir and East Rift Zone regions, and at 1–3 km depth, around the shallower Halema'uma'u reservoir, precede the 2018 LERZ eruption. The red arrows show the possible magma overturn at the summit and the transport in the LERZ during the dike intrusion. The question marks highlight the possible storage of the Pu'u'ō'ō olivine in the East Rift Zone during the 2018 LERZ eruption and possible connections in the ERZ. The moderately mafic melts (~7–7.5 MgO for Halema'uma'u shallow reservoir) fractionate progressively in the ERZ (~6.5 MgO at Pu'u'ō'ō prior to 2018; Gansecki et al., 2019). Older stored magmas with lower Fo olivine ($Fo_{70–75}$) were involved during the phase 1 of the 2018 LERZ eruption.

of Pu'u'ō'ō in May 2018. The variations in Sc cannot be simply related to clinopyroxene fractionation before olivine crystallization, since olivine is replaced by orthopyroxene as the liquidus phase at greater depth (beyond 0.4 GPa; Lynn et al., 2017). The variations in Sc in olivine are therefore likely inherited from the mantle source.

Mn/Sc ratios (Fig. 4d) provide a means to discriminate between lower Fo ($Fo_{<83}$) olivine from Pu'u'ō'ō, Halema'uma'u or LERZ 2018. Mn/Sc ratios in Pu'u'ō'ō olivine vary between 180 to 240. Low-Fo olivine ($Fo_{<83}$) from Halema'uma'u have similar Mn/Sc ratios (180 - 275) to Pu'u'ō'ō olivine. In contrast, $Fo_{<83}$ olivine from the LERZ 2018, have higher Mn/Sc ratios (from 250 to 400). About 27% of $Fo_{<83}$ olivine from LERZ 2018 have Mn/Sc ratios overlapping with those from Halema'uma'u, but no LERZ 2018 olivine has the same Mn/Sc ratio as Pu'u'ō'ō olivine. The large variability of the Mn/Sc values in 2018 LERZ olivine (Fig. 4d) may arise from mixing of olivine from various periods in a complex mush pile, partial diffusive re-equilibration and/or mixing between olivine crystallized from olivine-only magma (MgO > 7 wt.%) and olivine from plagioclase and pyroxene-bearing magma (MgO < 7 wt.%).

Although magmas feeding Pu'u'ō'ō from the summit could have been erupted in 2018, there's no evidence for magmas crystallizing at shallow depths immediately below Pu'u'ō'ō being drawn back into the plumbing system and erupted downrift. The fraction of Pu'u'ō'ō magma with olivine crystallizing at shallow levels potentially never reached the LERZ 2018 eruption site and may have instead been stored in a shallower part of the rift zone after the vent collapsed, or filled in available space during unzipping of the rift zone. The 2018 LERZ mafic magma, with its compositionally diverse olivine cargo, most likely originated from the summit reservoirs where primitive melts (up to 14 wt.% MgO; Gansecki et al., 2019; Lerner et al., 2021a; Wieser et al., 2021) mixed with lower MgO (< 7.5 wt. %) melts. More specifically, several lines of evidence identify the deeper South Caldera reservoir as an important source of mafic magma for the LERZ 2018 eruption. First, the summit caldera collapse and geophysical modeling based on pre- and syn-eruptive deformation argue that a large volume (>1 km^3) of magma was evacuated from one or both of the summit reservoirs (Anderson et al., 2019). Second, pre-eruptive seismicity showed several swarms in the months prior to May 2018 that are distributed around the inferred South Caldera storage region and could correspond to arrival of high-Fo olivine bearing primitive melts (Fig. 5; Flinders et al., 2020). Third, trace elements (Mn, Sc) in LERZ 2018 olivine only overlap with compositions from the summit reservoirs (Fig. 4a,d). But because olivine from the Halema'uma'u lava lake is, for the most part, different from LERZ olivine (>70% of Mn/Sc values not overlapping), the most likely origin for the dominant fraction of LERZ 2018 olivine is the deeper South Caldera reservoir. This interpretation fits generally well with storage configurations proposed based on melt inclusion entrapment depths. Lerner et al., 2021a and Wieser et al., 2021 found that most $<Fo_{86}$ olivine crystallized at shallow depths (typical of the Halema'uma'u reservoir), and that $Fo_{86–90}$ olivine could have formed in both Halema'uma'u and South Caldera reservoirs. The notable difference in Sc concentration between most of the LERZ 2018 olivine and Halema'uma'u 2008–2018 olivine provides an additional information: both low- and high-Fo LERZ

2018 olivines were for the most part sourced from South Caldera. This revised configuration contrasts slightly with the model proposed by Wieser et al. (2021) where most of the high-Fo olivine is inherited from South Caldera and low-Fo populations from the shallower Halema'uma'u system. Pietruszka et al. (2021) recently proposed, based on whole rock chemistry, that much of the LERZ 2018 mafic magma was derived from an accumulation zone east of Pu'u'ō'ō. The general absence of cumulate textures (e.g., kink bands, Gansecki et al., 2019) and the highly euhedral 'primary' nature of LERZ 2018 olivine morphologies precludes involvement of old, cold, compacted cumulate regions as suggested by Pietruszka et al., 2021. Thus, if the mafic magma had originated from the ERZ, the high- and low-Fo olivine cargo would have accumulated in this region in the decade preceding the eruption, as the reservoir was accumulating enough magma. Preservation of Fe-Mg in high-Fo olivine from diffusive re-equilibration for such long periods, however, are unlikely at magmatic temperatures corresponding to a ~7–7.5 wt.% MgO melt (Thomson and Maclennan, 2013; Mourey and Shea, 2019; Gordeychik et al., 2020), which precludes long residence of those crystals in the ERZ. Alternatively, a thermo-compositional gradient in the ERZ conduit caused by olivine settling could produce low- and high-Fo crystals, and where cooling at the floor and roof of the sill would create an asymmetric reservoir with high-Fo crystals in equilibrium with MgO-rich melts (Pankhurst et al., 2018).

The presence of compositionally distinct olivine populations between 2008 and 2018 within the South Caldera – Halema'uma'u summit reservoir system (Fig. 4b) has additional implications for the survival of multi-generational olivine populations in a mush pile (Thomson and Maclennan, 2013). Wieser et al., 2019 postulated, based on the variability of trace element ratios (Nb/Y) in melt inclusions from 20th century eruptions, that mush piles in summit reservoirs accumulate olivine from periods spanning decades to centuries. Scavenging of these cumulates and mush piles would occur during most eruptions, yielding compositionally variable melt inclusions. However, the relatively narrow Sc and Mn variations in the summit-derived 2018 high-Fo olivine cores and their distinct composition to 2008 summit olivine rules out the notion that primitive olivine represents century-old cumulates/mush. Instead, the high-Fo olivine studied here largely represent recently formed crystal cargo, with residence times of a decade or less, based on the time taken to diffusively homogenize whole olivine grains. Even lower Fo olivine populations (Fo_{78-82}) appear to lie on the Sc-Fo fractional crystallization trends outlined by their high-Fo counterparts, though with more variability in the case of 2018 LERZ (Fig. 4a). Hence, most low-Fo crystals are younger than a few decades in the eruptions investigated.

Based on the differences in Fo and Sc contents observed in the Halema'uma'u, Pu'u'ō'ō, and 2018 LERZ olivine, we propose a revised plumbing configuration that integrates petrological, geophysical and surface observations for the period 2008–2018 with three different olivine populations and for the syn-eruption period with three additional olivine populations (Fig. 5). The concordant trend in Sc in olivine from Halema'uma'u and Pu'u'ō'ō over the period 2008–2018 (Fig. 4a and b) confirms that the two reservoirs were directly connected in the years preceding the 2018 crisis (Patrick et al., 2020). By contrast, South Caldera-derived olivine erupted at LERZ in 2018 show no overlap in Sc content with Pu'u'ō'ō, implying that there was no direct connection between the two systems without passing through Halema'uma'u reservoir. As a result, before 2018, primitive magma (14 wt.% MgO, at equilibrium with Fo_{89-90}, and with 3.6–5.2 ppm Sc) was being fed from the deep crust to South Caldera where it likely mixed with a large volume of relatively mafic magma (MgO ~7.5 wt.%, Fo_{80-88}, Sc=3.9–7.5 ppm). This magma was transported towards Pu'u'ō'ō (MgO ~6.5–7 wt.%, Fo_{78-80}, Sc=8.4–10 ppm) after passage through Halema'uma'u (MgO ~7–7.5 wt.%, Fo_{80-82}, Sc=6.4–9.3 ppm).

Finally, the initial mixing event(s) between primitive melt and the LERZ 2018 mafic end-member (~7–7.5 wt.% MgO) was not preserved in the glass compositions of 2018 LERZ samples, which only increase in MgO from 5.5 to 7.2 wt.% during the high effusion rate phase of the eruption (Gansecki et al., 2019). Instead, syn-eruptive variations in MgO are chiefly associated with mixing of the ~7–7.5 wt.% mafic end-member and the two old evolved LERZ end-members. The input of primitive magma (MgO ~14 wt.%) is only recorded as high-Fo, euhedral olivine and their melt inclusions (Lerner et al., 2021a; Wieser et al., 2021). Such high-Fo olivine has occurred infrequently during the 20th and 21st centuries. We infer that primitive melts, which intrude the summit region of Kīlauea at a rate of ~0.1–0.2 km^3/yr (Poland et al., 2014; Wright and Klein, 2014), are a small fraction of the whole magma volume stored in the South Caldera reservoir, and thus are rapidly diluted into the much larger volume of resident melt. The presence of a large volume of relatively differentiated (~7–7.5 wt.% MgO) and primitive (up to ~14 wt.% MgO, crystallizing high-Fo olivine) magma in the South Caldera is thus a testament to the period of high magma supply and persistent, voluminous magma storage defining Kīlauea volcano since the 1950's (Wright and Klein, 2014; Poland et al., 2014).

3.2. Variability of primitive melts during the period 1500 – 2018

Olivine trace element compositions allowed us to establish the configuration and connectivity of the magmatic plumbing system underneath Kīlauea during the recent, dominantly effusive, eruptive period. Comparing the 2018 LERZ data with trace element data from the last explosive period (KT, 1500–1820), we next examine longer-term variations in olivine trace element compositions to better understand changes in primitive melt composition over the last explosive-effusive cycle. In particular, we evaluate processes underpinning the chemistry of high-Fo olivine: (1) fractional crystallization, (2) changes in source melting conditions (P, T, fO_2), (3) changes in the extent of melting (F), (4) changes in the composition of primary melts in the mantle source. Although most of the melting source parameters (T, P, F, X, fO_2) are not independent from each other, the next sections attempt to distinguish their related influences based on available petrological and geochemical indicators.

3.2.1. Influence of fractional crystallization

The Sc concentration of high-Fo olivine progressively decreases from 1500 to ~1820s and from 2008 to 2018, with a clear time progression within the KT spanning 320 years (8–13 ppm Sc in olivine; Fig. 4). High-Fo olivine from unit K1 and unit K2 have similar Sc contents. High-Fo olivine from the 2008 Halema'uma'u lava lake have slightly higher Sc contents than those from the LERZ 2018 eruption (~5.5–6.6 ± 0.25 ppm and ~3.6–5.2 ± 0.2 ppm, respectively). The substantial decrease in Sc contents in high-Fo olivine (~13 to 4 ppm) between the KT era and the recent decade of eruptions cannot be explained by fractional crystallization because Sc varies little with fractionation (Fig. 4a). In contrast, olivine Mn contents increased slightly from the 1500 to 2018 (Figs. 4b and 4c). Magma fractionation trends for Mn-in-olivine (as described in Putirka et al., 2018) with a starting liquid concentration with MnO = 0.17 wt% (peridotite type) with $K_{Mn}^{Ol/melt} = -3.6 + \frac{4500}{T(°C)}$ for lower temperature (and lower Fo, with 'K' the partition coefficient), and $K_{Mn}^{Ol/melt} = -6.2 + \frac{7800}{T(°C)}$ for higher-temperature (1150–1400 °C, higher Fo) can reproduce most of the LERZ 2018 olivine (Fo_{72-90}) Mn data but cannot reproduce the lower Mn contents of KT olivine (Fig. 4c). Thus, while fractional crystallization can cause changes in

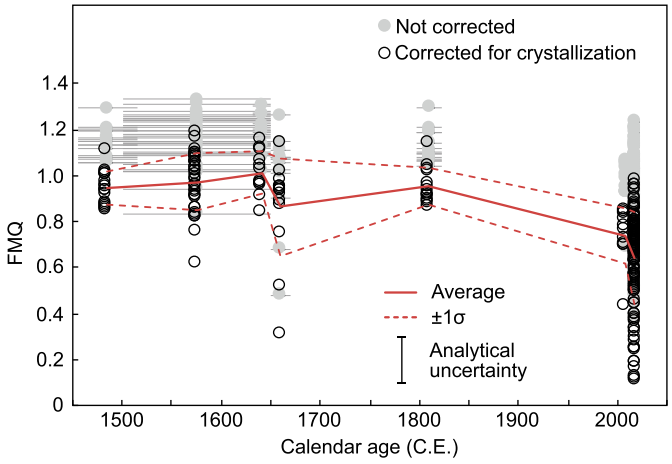

Fig. 6. Variations in oxygen fugacity reported as log units above the FMQ reaction buffer calculated from the V contents of primitive olivine (Fo>88) and V content in matrix glasses. The dashed lines are derived from the calibration in Canil, 2002. The V content in the matrix glass is corrected for olivine fractionation (see supplementary data for corrections), so that matrix glasses are plotted in equilibrium with the primitive olivine. Conditions were slightly more oxidized during the KT period than in 2008 at the Halema'uma'u lava lake. Slightly more reduced conditions are inferred for the LERZ 2018 eruption but could also reflect magma mixing during the eruption or greater sulfur degassing. Horizontal error bars correspond to the uncertainties on the eruption age for the KT units (from Swanson et al., 2012). Note that the calibration from Canil, 2002 of $K_V^{olivine/melt}$ is also function of temperature, melt composition and olivine composition. A lower temperature for a given fO_2 results in a higher 'K' value.

olivine Sc and Mn compositions for each individual eruption studied, variations between different eruptive periods must be induced through a different mechanism.

3.2.2. Influence of oxygen fugacity in the magma source region

The oxidation state of primitive Kīlauea magmas between 1500 and 2018 can be estimated using the V content in olivine and matrix glasses (Canil, 2002; Fig. 6). Here, we consider only the most forsteritic olivine (Fo>88 mol.%) to estimate the oxidation state close to the source. Measured V contents in matrix glasses were corrected for olivine fractionation using an initial primitive composition with 14 wt.% MgO (Lerner et al., 2021a, see calculations and V contents before and after corrections in the supplementary material). The calculated oxidation state for the KT period varies between FMQ +0.8 to +1.2. These fO_2 values are slightly lower than the hypothetical oxidized mantle plume inferred by Moussallam et al., 2019 (FMQ +1.5 to +2.5), but are higher than those obtained from gases and melt inclusions trapped at depth (FMQ +0.2 to +0.5; Moussallam et al., 2016), and similar to values retrieved from $Fe^{3+}/\Sigma Fe$ and $S^{6+}/\Sigma S$ ratios in Mauna Kea glasses (up to FMQ +0.9; Brounce et al., 2017). Vanadium-in-glass measurements of LERZ 2018 magmas indicate large variations in the oxidation state of primitive magmas (FMQ+0.1 to FMQ +1.0) consistent with recent measurements from melt inclusions (FMQ +0.5, Lerner et al., 2021b) and are slightly more reduced than KT magmas. However, some of the variations in the oxidation state in 2018 LERZ magmas could also reflect the influence of magma mixing between the mafic and more evolved stored magmas (e.g., Gansecki et al., 2019) on the final glass vanadium content used for our calculations. Thus, oxygen fugacity conditions may have changed by 0.4 log units in the last 500 years, but additional work examining V in high-Fo olivine hosted melt inclusions may be required to verify this.

3.2.3. Influence of primary melt source composition

First-row transition elements (e.g., Mn and Fe) in olivine are frequently used as tracers of chemical heterogeneities in the mantle and of variations in melting temperature or pressure (Sobolev et al., 2007; Le Roux et al., 2011). Partial melting of an upper mantle with olivine and orthopyroxene does not significantly fractionate Mn over Fe (Mallik et al., 2021). In contrast, the melting of a pyroxenitic mantle source with clinopyroxene and garnet should fractionate Mn from Fe. Hence, eclogite and pyroxenite melts have lower Mn/Fe ratios compared to peridotite melts (Humayun et al., 2004). Variable fractions of pyroxenite and peridotite can also reconcile the different Mn/Fe ratios and transition metal contents (e.g., Mn or Ni) in olivine (Sobolev et al., 2007; Wang and Gaetani, 2008). Our olivine data from the 1500-early 1820's KT and 2018 LERZ eruptions show variable Mn/Fe ratios at constant Ni/Mg ratios (Fig. 7a). Given that an increase in the olivine fraction in the melt source should increase Ni/Mg values, we instead attribute variations in Mn/Fe to a variation of the modal abundance of clinopyroxene in the source at the expanse of orthopyroxene between 1500 and 2018.

The two minerals that could cause Sc to decrease in Mg-rich olivine and their carrier primitive melts are garnet (representing 60% of the Sc budget of lherzolite; Chassé et al., 2018) and clinopyroxene (the most Sc-enriched mineral after garnet, accounting for 10% of the Sc budget in lherzolite). However, Mn is highly compatible in garnet ($K_{Mn}^{Gt/melt} \sim 3$, see supplementary for the references used for the choice of partition coefficients), while it is slightly incompatible in clinopyroxene ($K_{Mn}^{Cpx/melt} \sim 0.7$). Therefore, the decrease in Sc in primitive olivine (>Fo_{87}) with increasing Mn also implies that the contribution of clinopyroxene in the melt increased drastically (from 11 to 67% using simple batch melting calculations, Fig. 8).

Furthermore, Ni/Co values greater than 20 in olivine are often thought to reflect a pyroxenite source component (Sobolev et al., 2007; Foley et al., 2013). Primitive olivine (Fo>87) from KT have high Ni/Co values (Fig. 7b) between 20 and 30 (and low 100*Mn/Fe between 1 and 1.3) compared to the 2018 olivine (Ni/Co~20–24), and, to a first order, consistent with a higher proportion of pyroxenite in the source. However, depletion in Co, rather than high Ni content, is responsible for the high Ni/Co observed in the KT primitive olivine relative to the 2018 LERZ olivine (Fig. 7d). This decoupling between Co and Ni contents is not easily explained by a decreasing pyroxenite component with time. Instead, the increase in Co since the KT period can also be successfully reproduced by increasing the proportion of clinopyroxene that melted in the source over time relative to the proportion of orthopyroxene (Co being less compatible in clinopyroxene compared to orthopyroxene; $K_{Co}^{Opx/melt} = 1.3$ and $K_{Co}^{Cpx/melt} = 1.06$). Finally, an increase of the contribution of clinopyroxene at the expense of orthopyroxene is also consistent with the Zn-Mn correlations in olivine (Fig. 8b) and the broadly constant Zn/Fe ratio (Fig. 7c) as $K_D^{Zn/Fe}$ are similar for orthopyroxene and clinopyroxene at a given temperature (Le Roux et al., 2011).

3.2.4. Influence of mantle melting temperature and pressure

The lower Mn (and Mn/Fe ratio) in high-Fo olivine in KT compared to recent Kīlauea eruptions could also result from an increase in the degree of partial melting at lower pressure or higher temperature (Matzen et al., 2017; Putirka et al., 2018) from the KT to 2018 LERZ eruptions. We tested these hypotheses using major element compositions of olivine-hosted melt inclusions. Mantle potential temperatures (Fig. 9a) were calculated using primitive melt inclusions with MgO > 10 wt.% (after post-entrapment corrections). The melt inclusion compositions include the KT period (Sides et al., 2014), some of the 20th century Kīlauea eruptions (Kīlauea Iki, Maunaulu; Sides et al., 2014) and the 2018 LERZ eruption (Lerner et al., 2021a; Wieser et al., 2021). Mantle temperature calculations were carried out using the model from Lee

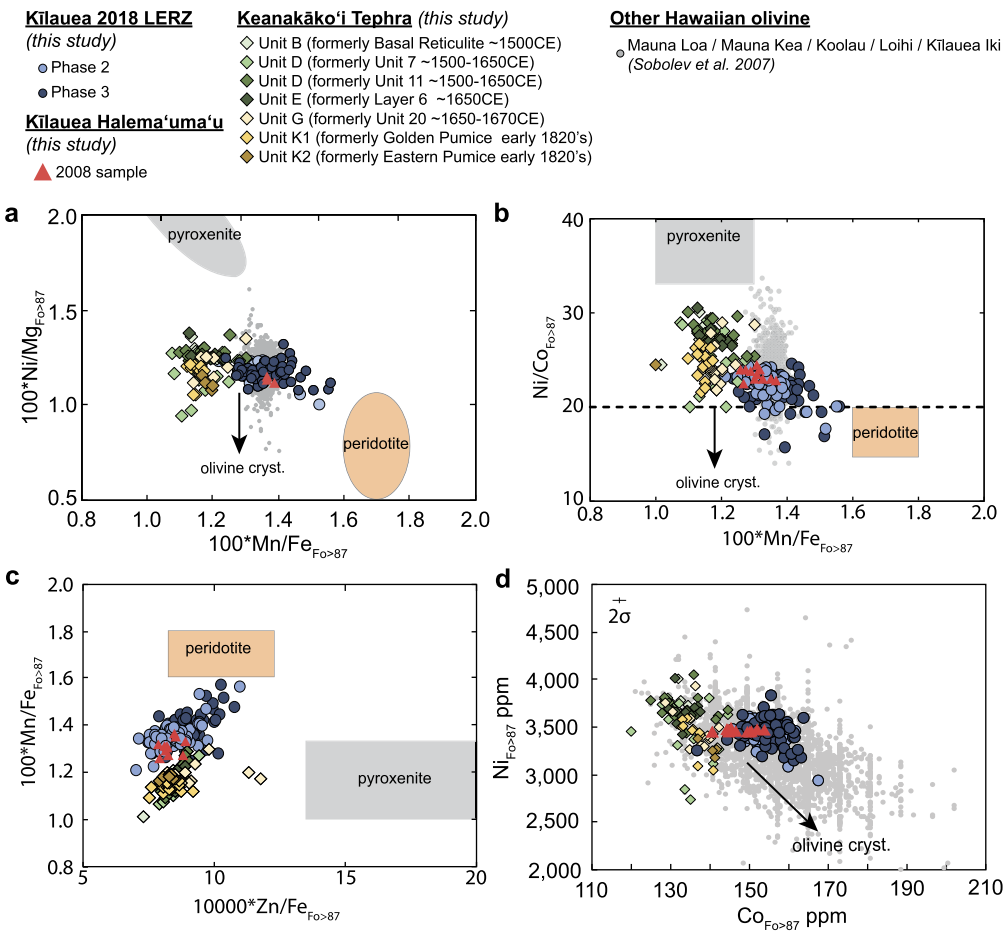

Fig. 7. Composition of Mg-rich (Fo>87) olivine phenocrysts for the 2018 LERZ, 2008 Halema'uma'u lava lake and ~1500–1820 KT period. (a) 100*Mn/Fe versus 100*Ni/Mg for primitive olivine (Fo>87) and fields for olivine in equilibrium with peridotite melts and pyroxenite melts (Sobolev et al., 2007). KT olivine are depleted in Mn compared to other Kīlauea olivine. (b) 100*Mn/Fe versus Ni/Co of primitive olivines (Fo>87). Ni/Co values >20 suggest a pyroxenitic component in the mantle source and Ni/Co~20 (value for the Bulk Silicate Earth) with 100*Mn/Fe between 1.6–1.8 would indicate a peridotite component (e.g., Sobolev et al., 2007; Foley et al., 2013). (c) 10000*Zn/Fe versus 100*Mn/Fe of primitive olivine (Fo>87). Fields of olivine in equilibrium with peridotite melts and pyroxenite melts are from the literature (Le Roux et al., 2010; Howarth and Harris, 2017). (d) Ni versus Co content in Fo>87 olivine. Black arrows in panel (a), (b) and (d) are illustrative trends for olivine crystallization.

et al., 2009 (with $K^{ol/melt}_{Fe^{2+}-Mg^{2+}} = 0.33$, Fo=92 mol.% in the mantle source and $Fe^{3+}/Fe_T = 0.18$; Lerner et al., 2021b). Because relative mean mantle temperature variations can be subtle (absolute values are subject to large and complex uncertainties), potential temperatures calculated for the 2018 LERZ eruption are statistically compared to the other eruptions using one-way analysis of variance (ANOVA) tests (Fig. 9a). The primitive melts supplying the 2018 LERZ eruption are found to be statistically slightly hotter (by around 10–15 °C) than the melts from the 20th century eruptions at Kīlauea (p-values 2×10^{-3} to 2×10^{-6}).

However, the increase in mean melting temperature is minor and within the error bars (~40 °C uncertainty) associated with these models (Lee et al., 2009). Also, different choice of initial FeO concentrations for post-entrapment corrections used in the studies (Sides et al., 2014; Lerner et al., 2021a; Wieser et al., 2021) can explain these differences in mantle potential temperature.

Mantle melting pressures for the KT, 2008 Halema'uma'u eruption, and the 2018 LERZ eruption are calculated from the same primitive melt inclusion compositions using the calibration from Lee et al., 2009 (Fig. 9b). We do not observe any major difference between the pressure calculated for the two eruptive periods, with mean mantle melting pressures of 2.5 ± 0.1 (1σ) GPa for the KT period and 2.6 ± 0.1 (1σ) GPa for the 2018 LERZ magmas.

To summarize, neither a change in the melting pressure or the mantle temperature can easily explain the clear variations observed in Sc, Mn, as well as the Ni/Mg and Mn/Fe ratios in primitive olivine. Instead, we suggest that these trace element variations are due to an increase in the fraction of clinopyroxene that melts in the mantle source. However, an increase in the degree of mantle fertility recorded within primitive melt compositions could also be associated with an increase in the degree of partial melting (for any degree of decompression and any fixed temperature) between the two eruptive periods (Hirschmann and Stolper, 1996). We next test this possibility using high-Fo olivine compositions.

3.2.5. Influence of degree of melting

De Hoog et al., 2010 proposed that the Cr# (= Cr/(Cr+Al) in mol) in primitive olivine (Fo>87) can be used to calculate the degree of melting (% $F_{melting} = 14.5 \times \ln Cr\#^{ol} + 26$). Only Fo>87 olivine cores (n=11 for Halema'uma'u 2008, n=111 for KT, n=147 for LERZ 2018) were used for these calculations to avoid issues related to diffusive re-equilibration of Cr at the rims. Using Cr data collected in olivine from the 2008 Halema'uma'u lava lake, 2018 LERZ and the KT eruptions, we find that the average degrees of partial melting in the source increased from 21.8% to 24% between 1500 and 2018 (i.e., a significant difference considering the 0.3% analytical uncertainties on these calculations; Fig. 10). These degrees of partial melting are comparable to those calculated by Putirka, 2016 (19%), but higher than those derived from incompatible trace elements (5–10% melting for lavas from the 19th and 20th centuries; Pietruszka and Garcia, 1999). Uncertainties related to the calibration are greater than the calculated variations in the

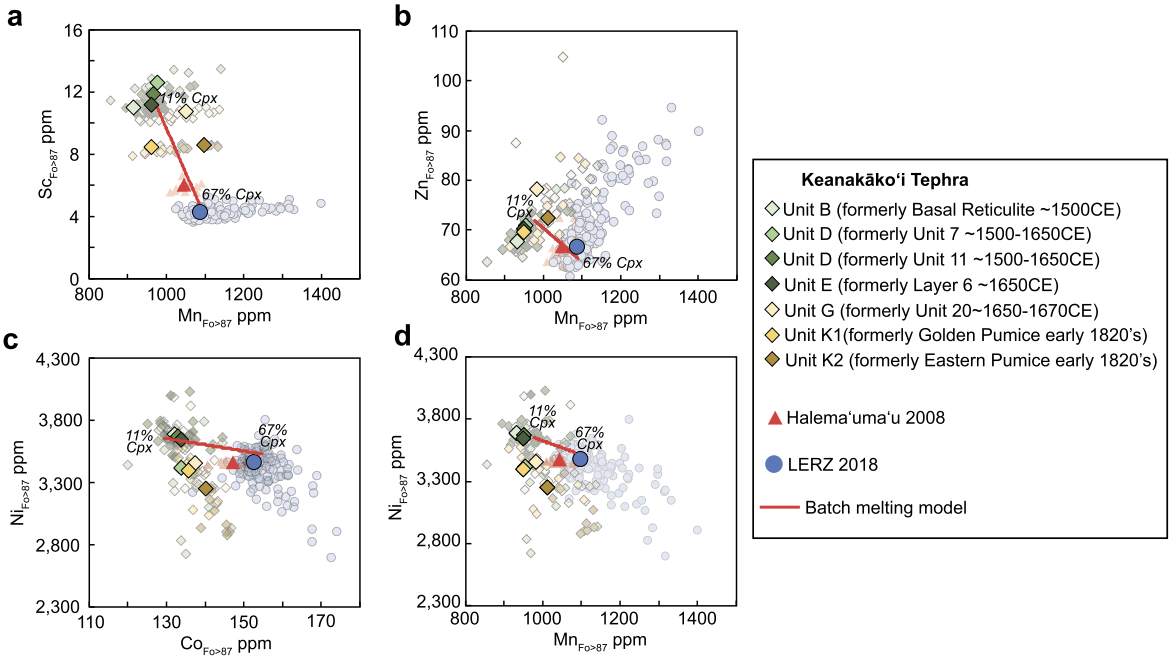

Fig. 8. Batch melting calculations for selected transition metals concentrations in forsteritic olivine (Fo>87). Best fit mantle lithology that participated in melting for KT magma is 6% olivine, 75% orthopyroxene, 11% clinopyroxene, 8% garnet. Best fit mantle lithology for 2018 LERZ magma is 4% olivine, 13% orthopyroxene, 67% clinopyroxene, 12% garnet, 4% spinel. This does not mean that these eruptions are necessary sourced from pyroxenites but means that the proportion of pyroxene that melted changed between 1500 and 2018. Full-color symbols are the averages for each eruption, faded background ones are all Fo>87 olivine data. (a) Sc versus Mn. Note that Sc is highly incompatible in spinel, while is highly compatible in garnet. Therefore, the decrease in Sc between 1500 and 2018 cannot be only explained by a switch from garnet- to spinel-field melting, since spinel counteract the contribution of clinopyroxene; (b) Zn versus Mn; (c) Ni versus Co; (d) Ni versus Mn.

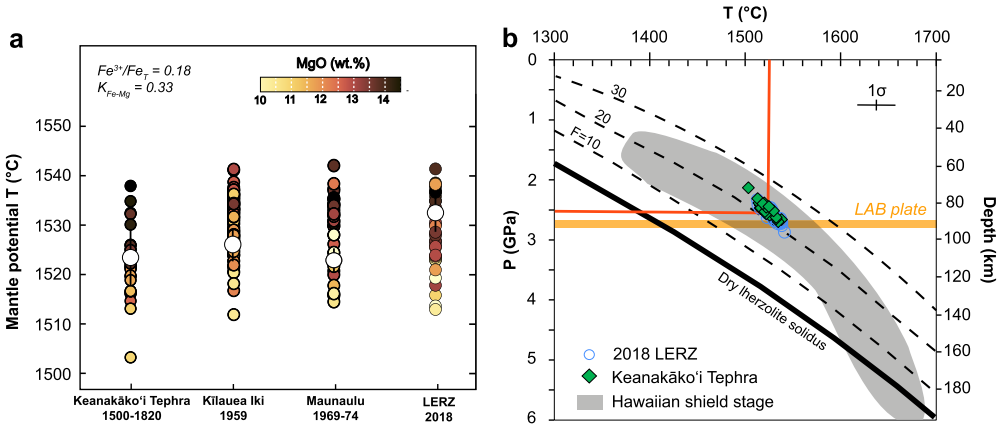

Fig. 9. Mean potential mantle temperatures and pressures calculated from KT and 2018 LERZ primitive melt inclusions (MgO>10wt.%). (a) Potential mantle temperature (Tp) calculated with primitive (MgO>10 wt.%) olivine-hosted melt inclusions compositions from different Kīlauea eruptions between 1500 and 2018. Tp were estimated using the parametrization from Lee et al., 2009. Melt inclusion data from KT, Kīlauea Iki and Maunaulu eruptions are from Sides et al., 2014 and melt inclusions from the 2018 LERZ eruption (fissure 8 'phase 3') are from Lerner et al., 2021a and Wieser et al., 2021. The temperatures calculated for the 2018 LERZ eruption are compared with the other eruptions using one-way analysis of variance (ANOVA tests; white circles represent the average and the bars represent the first and last quartile). The P- and F-values for the ANOVA tests are reported in supplementary data. (b) Pressures calculated from KT and 2018 LERZ primitive melt inclusions (MgO>10 wt.%). Temperatures and pressures calculated for Hawaiian shield basalts are from Lee et al., 2009. Curved dashed lines represent melting adiabats ('F' is the melting fraction; from Lee et al., 2009). Red lines are average pressure and temperature. Lithosphere-Asthenosphere Boundary (LAB) depth is from Dasgupta et al., 2010.

degree of melting, but this is a more qualitative approach in which we focus on the relative variation in degree of melting between the eruptive units. In any case, both degree of partial melting and source fertility (fraction of clinopyroxene inherited in primary melts) appear to have changed between the KT period and modern era.

3.3. Implications for eruptive cycles at Kīlauea

The difference in trace element concentrations in high-Fo olivine between the KT, 2008 Halema'uma'u and 2018 LERZ eruption periods provide key new insights into the long-term evolution of magma supply, storage and eruption at Kīlauea. Changes in the fraction of clinopyroxene that melts in the source, combined with an increase in melt productivity between 1500 and present day, are in excellent agreement with the observation that magma supply and eruption rates appear to have increased since the end of the KT era (Swanson et al., 2014; Wright and Klein, 2014; Lynn and Swanson, 2022). Clinopyroxene being the most fusible mineral in the mantle source, the increase in the degree of mantle fertility between 1500 and 2018 at a similar depth and temperature, may be explained by metasomatism (melt-rock interaction) that produce clinopyroxene-rich rocks in the mantle over the past century. Trace elements in melt inclusions and radiogenic isotopes (Pietruszka et

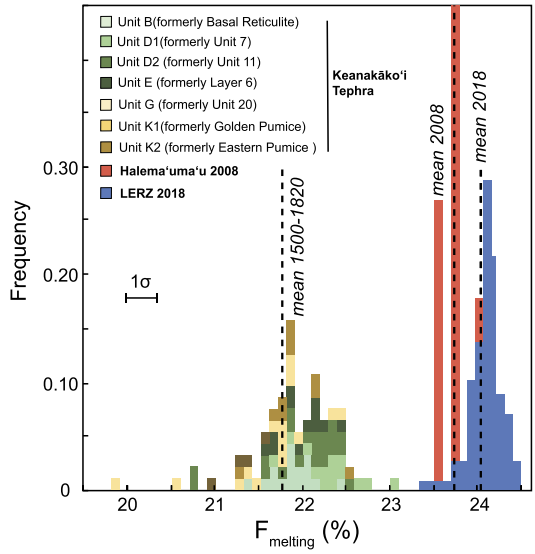

Fig. 10. Estimated degree of mantle partial melting for the 1500-early 1820's KT period, 2008 Halema'uma'u and 2018 LERZ magmas. The degree of partial melting (F) is estimated using the equation in De Hoog et al., 2010: $F_{melting} = 14.5 \times \ln(\text{Cr\#ol}) + 26(\text{Cr\#}$, molar ratio $\text{Cr}/(\text{Cr}+\text{Al}))$. Only high-Fo (Fo>87) olivine are used for these calculations. The 1500-early 1820's KT period was supplied by a lower degree of partial melting ($F \sim 21.7\%$) compared to the 2008 Halema'uma'u olivine ($F \sim 23.7\%$) or 2018 LERZ olivine ($F \sim 24\%$). One sigma analytical error (related to Cr# measurements) on $F_{melting}$ is ~0.3%. F values are only qualitative.

al., 1999; Sides et al., 2014) also underscore that magma supply from the mantle increased after the Kīlauea Iki eruption in 1959 in a trend that continued until 2018.

Changes in the supply of primitive magma to crustal reservoirs underneath Kīlauea are closely linked to variations in eruption style. Low magma supply tends to favor formation of ephemeral, less evolved, and perhaps more scattered magma reservoirs that erupt more primitive magmas with less stalling and crustal interaction (Lynn et al., 2017) while high magma supply tends to promote formation of large, steady and more evolved reservoirs (Lynn and Swanson, 2022). The change in the fraction of clinopyroxene and associated increase in partial melting in the mantle source may have contributed to the transition from dominantly explosive to dominantly effusive styles at Kīlauea. Higher magma supply during the 2008-present day effusive period at Kilauea is characterized by efficient mixing of primitive and stored magmas in shallow magma reservoirs. Shallow magma reservoirs may buffer ascending magmas and allow extensive degassing that reduces explosivity. In contrast, the absence of established mature shallow reservoir fed by lower magma supply during the Keanakako'i Tephra explosive period may have prevented magma degassing and therefore increase explosivity.

Petrologic monitoring of trace elements in olivine (in particular Sc) could help to recognize a decrease of mantle source productivity that might herald changes in magma supply and in the dominant eruptive style at Kīlauea. For instance, trends of increasing Sc in olivine with time could forewarn of a declining magma supply and a possible transition to a more explosive style at Kīlauea.

4. Conclusions

We compared olivine and olivine-hosted melt inclusion compositions from explosive Kīlauea eruptions (seven eruptions between 1500 and early 1820's from KT) and from effusive Kīlauea eruptions (Pu'u'ō'ō 2015–2018, Halema'uma'u 2008–2018, Halema'uma'u 2020 and LERZ 2018). This comparison revealed that:

1) Olivine from late-stage Pu'u'ō'ō (2015 to 2018) has different trace element compositions than olivine from the 2018 LERZ eruption. Sc contents in Fo_{78-80} Pu'u'ō'ō olivine are distinctly higher than Fo_{78-80} olivine from the 2018 LERZ eruption. This suggests that magma feeding Pu'u'ō'ō shortly prior to May 2018 played little role in the LERZ eruption and potentially remained stored in the rift zone after the collapse of Pu'u'ō'ō.

2) Mn and Sc contents in olivine indicate that most of the olivine cargo erupted in the 2018 LERZ magma is also different from the Halema'uma'u 2008–2018 olivine cargo, with only ~25% of the olivine analyzed having a composition overlapping the earlier Halema'uma'u samples.

3) The distinct Sc content of olivine erupted from the summit between 2008 and 2018 challenges the notion that multigenerational olivine cargo accumulated over centuries are amalgamated prior to major eruptions. Most of the LERZ 2018 olivine from the mafic magma end-member is likely decadal or less in age.

4) The decrease in Sc content combined with the increase in Mn content in primitive olivine (>Fo_{87}) between 1500 and 2018 implies that the proportion of clinopyroxene in the source increased drastically (from ~11 to 67%). There is no clear evidence of a significant change in mantle melting pressure or oxygen fugacity conditions between the two periods, although mantle melting temperature may have increased by 10–15 °C in the 21st century. The increase in clinopyroxene fraction in the melting reaction may also have been accompanied by an increase in the degree of melting from 1500 to 2018.

5) Sc in olivine may provide one of the most robust non-isotopic tracers of mantle source composition to date in Hawaiian magmas. Future studies focused on characterizing the partitioning and diffusivity of Sc in olivine will provide key constraints on why Sc in olivine appears to more faithfully record the chemical characteristics of primary magmas.

Olivine trace element data are also needed for the 1820–2008 period to confirm the trend in Sc content established by the KT and 2008–2018 olivine. Tracking the temporal evolution of these key trace elements in olivine from Hawai'i and elsewhere will allow characterizing changes in mantle source and magma supply histories, thereby tracking the long-term (hundreds to thousands of years) evolution of volcanic systems.

CRediT authorship contribution statement

Adrien J. Mourey: Conceptualization, Data curation, Investigation, Methodology, Writing – original draft. **Thomas Shea:** Funding acquisition, Writing – review & editing. **Kendra J. Lynn:** Data curation, Funding acquisition, Writing – review & editing. **Allan H. Lerner:** Investigation, Writing – review & editing. **Sarah Lambart:** Investigation, Writing – review & editing. **Fidel Costa:** Funding acquisition, Writing – review & editing. **Jeffrey Oalmann:** Data curation, Writing – review & editing. **R. Lopaka Lee:** Resources. **Cheryl Gansecki:** Resources.

Declaration of competing interest

The authors declare that they have no known competing financial interests or personal relationships that could have appeared to influence the work reported in this paper.

Data availability

All compositional data obtained in this study are included in the supplementary data tables.

Acknowledgements

We acknowledge Rosalind Helz for comments on a previous version of the manuscript. We thank Chiara Maria Petrone for edi-

torial handling, David Neave and an anonymous reviewer for critical reviews, and Jordan Lubbers for the USGS internal review. This work was supported by the National Science Foundation through a NSF EAR Grant 1725321 to TS and both an East Asia and Pacific Summer Institutes NSF grant (OISE-1513668) and the Fred M. Bullard Graduate Fellowship at the University of Hawai'i to KJL. Any use of trade, firm, or product names is for descriptive purposes only and does not imply endorsement by the U.S. Government.

Appendix A. Supplementary material

Supplementary material related to this article can be found online at https://doi.org/10.1016/j.epsl.2022.117769.

References

Anderson, K.R., Johanson, I.A., Patrick, M.R., Gu, M., Segall, P., Poland, M.P., Montgomery-Brown, E.K., Miklius, A., 2019. Magma reservoir failure and the onset of caldera collapse at Kīlauea Volcano in 2018. Science 366, 6470. https://doi.org/10.1126/science.aaz1822.

Bouvet de Maisonneuve, C., Costa, F., Huber, C., Vonlanthen, P., Bachmann, O., Dungan, M.A., 2016. How do olivines record magmatic events? Insights from major and trace element zoning. Contrib. Mineral. Petrol. 171, 1–20.

Brounce, M., Stolper, E., Eiler, J., 2017. Redox variations in Mauna Kea lavas, the oxygen fugacity of the Hawaiian plume, and the role of volcanic gases in Earth's oxygenation. Proc. Natl. Acad. Sci. 114, 8997–9002. https://doi.org/10.1073/pnas.1619527114.

Brigham, W.T., 1909. The Volcanoes of Kilauea and Mauna Loa on the Island of Hawaii. Memoirs of the Bernice Pauahi Bishop Museum, Vol. II, no. 4. Bishop Museum, Honolulu. 222 pp. Reprinted in 1974 by Kraus Reprint Co., Millwood, NY.

Canil, D., 2002. Vanadium in peridotites, mantle redox and tectonic environments: archean to present. Earth Planet. Sci. Lett. 195, 75–90. https://doi.org/10.1016/S0012-821X(01)00582-9.

Chassé, M., Griffin, W.L., Alard, O., O'Reilly, S.Y., Calas, G., 2018. Insights into the mantle geochemistry of scandium from a meta-analysis of garnet data. Lithos 310–311, 409–421. https://doi.org/10.1016/j.lithos.2018.03.026.

Dasgupta, R., Jackson, M.G., Lee, C.-T.A., 2010. Major element chemistry of ocean island basalts — conditions of mantle melting and heterogeneity of mantle source. Earth Planet. Sci. Lett. 289, 377–392. https://doi.org/10.1016/j.epsl.2009.11.027.

De Hoog, J.C.M., Gall, L., Cornell, D.H., 2010. Trace-element geochemistry of mantle olivine and application to mantle petrogenesis and geothermobarometry. Chem. Geol. 270, 196–215. https://doi.org/10.1016/j.chemgeo.2009.11.017.

Flinders, A.F., Caudron, C., Johanson, I.A., Taira, T., Shiro, B., Haney, M., 2020. Seismic velocity variations associated with the 2018 lower East Rift Zone eruption of Kīlauea, Hawai'i. Bull. Volcanol. 82 (6). https://doi.org/10.1007/s00445-020-01380-w.

Foley, S.F., Prelevic, D., Rehfeldt, T., Jacob, D.E., 2013. Minor and trace elements in olivines as probes into early igneous and mantle melting processes. Earth Planet. Sci. Lett. 363, 181–191. https://doi.org/10.1016/j.epsl.2012.11.025.

Gansecki, C., Lopaka Lee, R., Shea, T., Lundblad, S.P., Hon, K., Parcheta, C., 2019. The tangled tale of Kilauea's 2018 eruption as told by geochemical monitoring. Science 366, eaaz0147. https://doi.org/10.1126/science.aaz0147.

Gleeson, M.L.M., Gibson, S.A., 2019. Crustal controls on apparent mantle pyroxenite signals in ocean island basalts. Geology 47 (4), 321–324. https://doi.org/10.1130/G45759.1.

Gordeychik, B., Churikova, T., Shea, T., Kronz, A., Simakin, A., Wörner, G., 2020. Fo and Ni relations in olivine differentiate between crystallization and diffusion trends. J. Petrol. 61, egaa083.

Helz, R.T., Clague, D.A., Sisson, T.W., Thornber, C.R., 2014. Petrologic insights into basaltic volcanism at historically active Hawaiian volcanoes. In: Poland, Kauahikaua (Eds.), Characteristics of Hawaiian Volcanoes, USGS Prof. Pap. 1801, 6, pp. 1–55.

Hirschmann, M.M., Stolper, E.M., 1996. A possible role for garnet pyroxenite in the origin of the "garnet signature" in MORB. Contrib. Mineral. Petrol. 124, 185–208.

Howarth, G.H., Harris, C., 2017. Discriminating between pyroxenite and peridotite sources for continental flood basalts (CFB) in southern Africa using olivine chemistry. Earth Planet. Sci. Lett. 475, 143–151. https://doi.org/10.1016/j.epsl.2017.07.043.

Humayun, M., Qin, L., Norman, M.D., 2004. Geochemical evidence for excess iron in the Mantle Beneath Hawaii. Science 306, 91–94. https://doi.org/10.1126/science.1101050.

Kern, C., Lerner, A.H., Elias, T., et al., 2020. Quantifying gas emissions associated with the 2018 rift eruption of Kīlauea Volcano using ground-based DOAS measurements. Bull. Volcanol. 82, 55. https://doi.org/10.1007/s00445-020-01390-8.

Lee, C.-T.A., Luffi, P., Plank, T., Dalton, H., Leeman, W.P., 2009. Constraints on the depths and temperatures of basaltic magma generation on Earth and other terrestrial planets using new thermobarometers for mafic magmas. Earth Planet. Sci. Lett. 279, 20–33. https://doi.org/10.1016/j.epsl.2008.12.020.

Le Roux, V., Lee, C.-T.A., Turner, S.J., 2010. Zn/Fe systematics in mafic and ultramafic systems: Implications for detecting major element heterogeneities in the Earth's mantle. Geochim. Cosmochim. Acta 74, 2779–2796. https://doi.org/10.1016/j.gca.2010.02.004.

Le Roux, V., Dasgupta, R., Lee, C.-T.A., 2011. Mineralogical heterogeneities in the Earth's mantle: constraints from Mn, Co, Ni and Zn partitioning during partial melting. Earth Planet. Sci. Lett. 307, 395–408. https://doi.org/10.1016/j.epsl.2011.05.014.

Lerner, A.H., Wallace, P.J., Shea, T., Mourey, A.J., et al., 2021a. The petrologic and degassing behavior of sulfur and other magmatic volatiles from the 2018 eruption of Kīlauea, Hawai'i: melt concentrations, magma storage depths, and magma recycling. Bull. Volcanol. 83, 43. https://doi.org/10.1007/s00445-021-01459-y.

Lerner, A.H., Muth, M.J., Wallace, P.J., Lanzirotti, A., Newville, M., Gaetani, G.A., Chowdhury, P., Dasgupta, R., 2021b. Improving the reliability of Fe- and S-XANES measurements in silicate glasses: correcting beam damage and identifying Fe-oxide nanolites in hydrous and anhydrous melt inclusions. Chem. Geol. 586, 120610. https://doi.org/10.1016/j.chemgeo.2021.120610.

Lynn, K.J., Garcia, M.O., Shea, T., Costa, F., Swanson, D.A., 2017. Timescales of mixing and storage for Keanakāko'i Tephra magmas (1500–1820 C.E.), Kīlauea Volcano, Hawai'i. Contrib. Mineral. Petrol. 172 (9). https://doi.org/10.1007/s00410-017-1395-4.

Lynn, K.J., Garcia, M.O., Shea, T., 2020. Phosphorus coupling obfuscates lithium geospeedometry in olivine. Front. Earth Sci. 8, 135. https://doi.org/10.3389/feart.2020.00135.

Lynn, K.J., Swanson, D.A., 2022. Olivine and glass chemistry record cycles of plumbing system recovery after summit collapse events at Kīlauea Volcano, Hawai'i. J. Volcanol. Geotherm. Res. 426, 107540.

Mallik, A., Lambart, S., Chin, E.J., 2021. Tracking the evolution of magmas from heterogeneous mantle sources to eruption. In: Mantle Convection and Surface Expressions, pp. 151–177.

Mallmann, G., O'Neill, H.St.C., 2009. The crystal/melt partitioning of V during mantle melting as a function of oxygen fugacity compared with some other elements (Al, P, Ca, Sc, Ti, Cr, Fe, Ga, Y, Zr and Nb). J. Petrol. 50, 1765–1794. https://doi.org/10.1093/petrology/egp053.

Matzen, A.K., Baker, M.B., Beckett, J.R., Stolper, E.M., 2011. Fe–Mg partitioning between olivine and high-magnesian melts and the nature of Hawaiian parental liquids. J. Petrol. 52, 1243–1263. https://doi.org/10.1093/petrology/egq089.

Matzen, A.K., Wood, B.J., Baker, M.B., Stolper, E.M., 2017. The roles of pyroxenite and peridotite in the mantle sources of oceanic basalts. Nat. Geosci. 10, 530–535.

McPhie, J., Walker, J.P., Christiansen, R.L., 1990. Phreatomagmatic and phreatic fall and surge deposits from explosions at Kilauea volcano, Hawaii, 1790 A.D.: Keanakakoi Ash Member. Bull. Volcanol. 52, 334–354. https://doi.org/10.1007/BF00302047.

Mourey, A.J., Shea, T., 2019. Forming olivine phenocrysts in basalt: a 3D characterization of growth rates in laboratory experiments. Front. Earth Sci. 7.

Moussallam, Y., Edmonds, M., Scaillet, B., Peters, N., Gennaro, E., Sides, I., Oppenheimer, C., 2016. The impact of degassing on the oxidation state of basaltic magmas: a case study of Kīlauea Volcano. Earth Planet. Sci. Lett. 450, 317–325. https://doi.org/10.1016/j.epsl.2016.06.031.

Moussallam, Y., Longpré, M.-A., McCammon, C., Gomez-Ulla, A., Rose-Koga, E.F., Scaillet, B., Peters, N., Gennaro, E., Paris, R., Oppenheimer, C., 2019. Mantle plumes are oxidised. Earth Planet. Sci. Lett. 527, 115798.

Neal, C.A., et al., 2019. The 2018 rift eruption and summit collapse of Kilauea volcano. Science 363, 367–374. https://doi.org/10.1126/science.aav7046.

Nikkola, P., Guðfinnsson, G.H., Bali, E., Rämö, O.T., Fusswinkel, T., Thordarson, T., 2019. Signature of deep mantle melting in South Iceland olivine. Contrib. Mineral. Petrol. 174 (5). https://doi.org/10.1007/s00410-019-1580-8.

Pankhurst, M.J., Morgan, D.J., Thordarson, T., Loughlin, S.C., 2018. Magmatic crystal records in time, space, and process, causatively linked with volcanic unrest. Earth Planet. Sci. Lett. 493, 231–241. https://doi.org/10.1016/j.epsl.2018.04.025.

Paton, C., Hellstrom, J., Paul, B., Woodhead, J., Hergt, J., 2011. Iolite: freeware for the visualisation and processing of mass spectrometric data. J. Anal. At. Spectrom. 26, 2508. https://doi.org/10.1039/c1ja10172b.

Patrick, M.R., Houghton, B.F., Anderson, K.R., et al., 2020. The cascading origin of the 2018 Kīlauea eruption and implications for future forecasting. Nat. Commun. 11, 5646. https://doi.org/10.1038/s41467-020-19190-1.

Pietruszka, A.J., Garcia, M.O., 1999. A rapid fluctuation in the mantle source and melting history of Kilauea Volcano inferred from the geochemistry of its historical summit lavas (1790–1982). J. Petrol. 40, 1321–1342. https://doi.org/10.1093/petroj/40.8.1321.

Pietruszka, A.J., Garcia, M.O., Rhodes, J.M., 2021. Accumulated PuʻuʻŌʻō magma fed the voluminous 2018 rift eruption of Kīlauea Volcano: evidence from lava chemistry. Bull. Volcanol. 83, 59. https://doi.org/10.1007/s00445-021-01470-3.

Poland, M.P., Miklius, A., Jeff Sutton, A., Thornber, C.R., 2012. A mantle-driven surge in magma supply to Kīlauea Volcano during 2003–2007. Nat. Geosci. 5 (4), 295–300. https://doi.org/10.1038/ngeo1426.

Poland, M.P., Miklius, A., Montgomery-Brown, E.K., 2014. Magma supply, storage, and transport at shield-stage Hawaiian volcanoes. USGS Prof. Pap. 1801. pp. 179–234.

Putirka, K., 2016. Rates and styles of planetary cooling on Earth, Moon, Mars, and Vesta, using new models for oxygen fugacity, ferric-ferrous ratios, olivine-liquid Fe-Mg exchange, and mantle potential temperature. Am. Mineral. 101, 819–840. https://doi.org/10.2138/am-2016-5402.

Putirka, K., Tao, Y., Hari, K.R., Perfit, M.R., Jackson, M.G., Arevalo, R., 2018. The mantle source of thermal plumes: trace and minor elements in olivine and major oxides of primitive liquids (and why the olivine compositions don't matter). Am. Mineral. 103, 1253–1270. https://doi.org/10.2138/am-2018-6192.

Sides, I.R., Edmonds, M., Maclennan, J., Swanson, D.A., Houghton, B.F., 2014. Eruption style at Kīlauea Volcano in Hawai'i linked to primary melt composition. Nat. Geosci. 7, 464–469. https://doi.org/10.1038/ngeo2140.

Sobolev, A.V., Hofmann, A.W., Kuzmin, D.V., Yaxley, G.M., Arndt, N.T., Chung, S.-L., Garcia, M.O., Gurenko, A.A., Danyushevsky, L.V., Elliott, T., Frey, F.A., Kamenetsky, V.S., Kerr, A.C., Krivolutskaya, N.A., Matvienkov, V.V., Nikogosian, I.K., Rocholl, A., Suschevskaya, N.M., Teklay, M., 2007. The amount of recycled crust in sources of mantle derived melts. Science 316, 412–417.

Spandler, C., O'Neill, H.S.C., 2010. Diffusion and partition coefficients of minor and trace elements in San Carlos olivine at 1300 °C with some geochemical implications. Contrib. Mineral. Petrol. 159, 791–818.

Swanson, D.A., Rose, T.R., Fiske, R.S., McGeehin, J.P., 2012. Keanakāko'I Tephra produced by 300 years of explosive eruptions following collapse of Kīlauea's caldera in about 1500 CE. J. Volcanol. Geotherm. Res. 215–216, 8–25. https://doi.org/10.1016/j.jvolgeorres.2011.11.009.

Swanson, D.A., Rose, T.R., Mucek, A.E., Garcia, M.O., Fiske, R.S., Mastin, L.G., 2014. Cycles of explosive and effusive eruptions at Kīlauea Volcano, Hawai'i. Geology 42, 631–634. https://doi.org/10.1130/G35701.1.

Swanson, D.A., Houghton, B.F., 2018. Products, processes, and implications of Keanakāko'i volcanism, Kılauea Volcano, Hawai'i. In: Poland, M.P., Garcia, M.O., Camp, V.E., Grunder, A. (Eds.), Field Volcanology: a Tribute to Disting Career Don Swanson. In: Geol. Soc. Am. Spec. Pap., vol. 538, pp. 159–190.

Thomson, A., Maclennan, J., 2013. The distribution of olivine compositions in Icelandic basalts and picrites. J. Petrol. 54, 745–768.

Wang, Z., Gaetani, G.A., 2008. Partitioning of Ni between olivine and siliceous eclogite partial melt: experimental constraints on the mantle source of Hawaiian basalts. Contrib. Mineral. Petrol. 156, 661–678. https://doi.org/10.1007/s00410-008-0308-y.

Wieser, P.E., Edmonds, M., Maclennan, J., et al., 2019. Crystal scavenging from mush piles recorded by melt inclusions. Nat. Commun. 10, 5797. https://doi.org/10.1038/s41467-019-13518-2.

Wieser, P.E., Lamadrid, H., Maclennan, J., Edmonds, M., Matthews, S., Iacovino, K., Jenner, F.E., Gansecki, C., Trusdell, F., Lee, R.L., Ilyinskaya, E., 2021. Reconstructing magma storage depths for the 2018 Kīlauean eruption from melt inclusion CO2 contents: the importance of vapor bubbles. Geochem. Geophys. Geosyst. 22, e2020GC009364. https://doi.org/10.1029/2020GC009364.

Wright, T.L., Klein, F.W., 2014. Two Hundred Years of Magma Transport and Storage at Kīlauea Volcano, Hawai'i, 1790–2008. USGS Prof. Pap. 1806. pp. 1–240.